Highlights

Solid-State MAS NMR at Ultra Low Temperature of Hydrated Alanine Doped with DNP Radicals

Yuanxin Li, Raj Chaklashiya, Hiroki Takahashi, Yoshifumi Kawahara, Kan Tagami, Celeste Tobar, Songi Han

- A closed-cycle He MAS system provides stable MAS at ULT without He leakage.
- At 25 K, ^{1}H NMR was observed with 4-fold intensity gain compared to at 100 K.
- ULT NMR provides greater benefit by allowing efficient CP in methyl group moieties.
- ^{1}H T_1 is dramatically shortened from minutes to seconds by adding CE DNP radicals.
- By adding CE radicals, the CH_3 ^{13}C linewidth barely increased at ULT.

Solid-State MAS NMR at Ultra Low Temperature of Hydrated Alanine Doped with DNP Radicals

Yuanxin Li[a], Raj Chaklashiya[b], Hiroki Takahashi[c], Yoshifumi Kawahara[d], Kan Tagami[a], Celeste Tobar[a], Songi Han[a,e]

[a]*Department of Chemistry and Biochemistry University of California Santa Barbara Santa Barbara California 93106 United States.*
[b]*Materials Department University of California Santa Barbara Santa Barbara California 93106 United States.*
[c]*JEOL RESONANCE Inc. Japan*
[d]*Cryovac Corp. Japan*
[e]*Department of Chemical Engineering University of California Santa Barbara Santa Barbara California 93106 United States.*

Abstract

Magic angle spinning (MAS) nuclear magnetic resonance (NMR) experiments at ultra low temperature (ULT) ($\ll$ 100 K) have demonstrated clear benefits for obtaining large signal sensitivity gain and probing spin dynamics phenomena at ULT. ULT NMR is furthermore a highly promising platform for solid-state dynamic nuclear polarization (DNP). However, ULT NMR is not widely used, given limited availability of such instrumentation from commercial sources. In this paper, we present a comprehensive study of hydrated [U-^{13}C]alanine, a standard bio-solid sample, from the first commercial 14.1 Tesla NMR spectrometer equipped with a closed-cycle helium ULT-MAS system. The closed-cycle helium MAS system provides precise temperature control from 25 K to 100 K and stable MAS from 1.5 kHz to 12 kHz. The ^{13}C CP-MAS NMR of [U-^{13}C]alanine showed 400% signal gain at 28 K compared with at 100 K. The large sensitivity gain results from the Boltzmann factor, radio frequency circuitry quality factor improvement, and the suppression of its methyl group rotation at ULT. We further observed that the addition of organic biradicals widely used for solid-state DNP significantly shortens the ^{1}H T_1 spin lattice relaxation time at ULT, without further broadening the ^{13}C spectral linewidth compared to at 90 K. The mechanism of ^{1}H T_1 shortening is dominated by the two-electron-one-nucleus triple flip transition underlying the Cross Effect mechanism, widely relied upon to drive

solid-state DNP. Our experimental observations suggest that the prospects of MAS NMR and DNP under ULT conditions established with a closed-cycle helium MAS system are bright.

Keywords: Dynamic Nuclear Polarization, ULT NMR, ULT DNP, closed-cycle helium circulation
PACS: 0000, 1111
2000 MSC: 0000, 1111

---

1. Introduction

Solid-state magic angle spinning (MAS) nuclear magnetic resonance (NMR) is an essential tool for the study of inorganic and biological solid samples. However, NMR has intrinsically low signal sensitivity, and hence instrument and methods developments to enhance MAS NMR sensitivity are ongoing efforts. There has been much progress in improving the MAS NMR sensitivity by increasing the magnetic field B_0,[1, 2] lowering the sample temperature,[3, 4, 5, 6, 7, 8, 9] cooling the radio frequency (RF) circuitry,[10, 11] applying efficient cross-polarization (CP) from abundant ^{1}H nuclear spins, shortening the experimental repetition time by adding paramagnetic dopants [12, 13], and by hyperpolarization techniques, most commonly dynamic nuclear polarization (DNP).[3, 4, 5, 14] Performing DNP-enhanced MAS NMR at high B_0 integrated with sample cooling to ultra low temperature (ULT, $\ll$ 100 K) can yield signal sensitivity gain by potentially several thousand fold compared with room temperature MAS NMR without DNP at the same field. However, there are theoretical and technical challenges to routinely achieving ULT NMR operation. Moreover, NMR line broadening and increasing nuclear spin lattice relaxation time (T_1) are major concerns with performing ULT NMR experiments.

The minimum sample temperature largely depends on the cooling gas used in the MAS NMR system. Generally speaking, three types of gases have been used to achieve low temperature NMR: 1) dried air ($\sim$ 250 K to room temperature); 2) nitrogen cooled to liquid nitrogen temperature ($\geq$ 77 K); and 3) helium cooled by compressors and/or liquid helium ($<$ 77 K). MAS NMR cooled by cold nitrogen gas to 110-80 K has been used to study the structural properties of vitrified proteins in solution or trapped transient states of proteins.[15, 16, 17] However, there is significant interest in pushing

the sample temperature further down to the ULT regime for the study of systems whose key dynamical properties, including methyl group rotations and ring flips, at ULT are of interest and/or for maximizing DNP enhanced NMR sensitivity. An ideal ULT MAS NMR system achieves efficient cooling, stable low temperature, stable MAS, no helium consumption, easy sample exchange, easy operation and little maintenance effort.

There have been persistent interest and endeavors in the development of helium cooled systems to achieve ULT NMR/DNP. The journey began in the 1980s when Yannoni and co-workers successfully conducted ^{13}C Cross Polarization (CP)-MAS NMR experiments at ULT on several organic molecules and polymers using cold helium gas directly warmed up from liquid helium for spinning and cooling.[18, 19] A maximum sample spinning speed of 2.5 kHz and a minimum sample temperature of 4.2 K was achieved, however with a large liquid helium consumption rate (15 L/h at 30 K with 1 kHz MAS). In 1997, the Griffin group at MIT adapted the Yannoni design and combined the ULT NMR with DNP capabilities at 5 T. [3] A significant increase in the DNP enhancement was achieved at 25 K ($\sim$ 100) compared with 100 K ($\sim$ 5). New designs and optimizations have been implemented to further increase the MAS frequency at ULT. Samoson *et al.* customized a ULT MAS NMR system located in Tallinn to allow $\leq$ 20 kHz MAS at $\geq$ 7 K with a 2 mm rotor.[20] In the Tallinn design, helium is used in all three gas lines (bearing, drive, and VT), and is later recovered and recycled. The main problems of the Tallinn design, however, were the limited stability and that the sample temperature is strongly coupled to the MAS rate. The Levitt group provided another design in Southampton using super-critical helium in a pressurized vessel for the three gas lines. [21] The super-critical helium avoids the instability caused by the inherent two-phase flow of liquid helium and the Levitt design allowed for a minimum sample temperature of 9.6 K with 15 kHz MAS using a 2 mm rotor. However, the current operation of the Southampton system using the super-critical helium generator is expensive due to large demand for liquid helium ($\sim$5000 L). The Barnes group customized their own cryostat in order to integrate it with a versatile MAS DNP probe and rotor design.[6] The Barnes design uses liquid helium for cooling and spinning, and hence requires a large liquid helium consumption rate of $\sim$33 L/h to achieve sample temperatures of $<$6 K. The Tycko group in Bethesda (NIH) developed an alternative approach, where cold helium gas is used only for cooling the sample and cold nitrogen gas is used for spinning.

This design allowed significant reduction in the liquid helium consumption rate of about 3 L/h and enabled MAS-DNP experiments at 20 K with ∼7 kHz MAS for a 4 mm rotor.[5] This design was later commercialized by Revolution NMR LLC and installed in the Han group at UC Santa Barbara.[22]

In order to further reduce the helium consumption rate, closed-cycle helium systems were designed to recover the helium used for cooling and spinning. The De Paëpe group at Grenoble designed a ULT MAS DNP system equipped with a helium circulation system and achieved up to 15 kHz MAS at 30 K using a 3.2 mm rotor. [7, 23] A spinning stability of 7 kHz ± 50 Hz was measured at 50 K.[7] In this design, the cryostat is initially cooled down to ∼80 K using liquid nitrogen. To achieve temperatures < 77 K, the cryostat was flushed with room temperature helium gas and then cooled using cold helium gas directly boiled off from a liquid helium dewar. The NMR/DNP probes are further cooled using recirculated pressurized bearing, drive, and VT helium gases cooled by the cryostat. The helium gas consumption rate for the Grenoble design is low at only ≪ 1 L/h for both the leaks and pneumatic rotor insertion/ejection. However, the current Grenoble design still consumes liquid helium at a relatively high rate of 5-25 L/h to maintain the cold temperature of the cryostat and the liquid helium consumption rate depends on the desired sample temperature and MAS. The next generation of fully autonomous system with zero liquid helium consumption is developed and under testing, as mentioned in the recent publications.[7, 23] Another closed-cycle helium circulation ULT NMR/DNP design has been introduced by the Fujiwara team in Osaka, where cold helium gas is used for bearing and drive (there is no VT channel in the design).[24, 25, 26, 27] It is worth noting that the Osaka design does not use liquid helium, which is a big improvement from all the other designs mentioned above. In the Osaka design, helium gas is initially cooled by vacuum insulated heat exchangers for both bearing and drive. The cold helium gas is pressurized by bellows compressors and the precise flow rate is further regulated using mass flow controllers. The regulated helium gas is then used for sample cooling and spinning. The return helium gas is still cold and hence can be used in the initial cooling step through a tube-in-tube type counter-flow heat exchanging system. This system has shown great stability in sample temperature and spinning, where 8 kHz of stable MAS at 20 K has been reported with only ± 5 Hz variations in the MAS speed after days of running using a 3.2 mm rotor.[4] In 2020, JEOL RESONANCE Inc. has commercialized the Osaka design and launched its

first installation in collaboration with the Han group at UC Santa Barbara.

ULT gives rise to large NMR signal sensitivity gain from both the Boltzmann factor and the general increase in the quality factor (Q), as well as the reduction of the Johnson-Nyquist noise (thermal noise) in the RF circuit. In addition, the capabilities of ULT MAS NMR can offer more profound scientific benefits. For example, through the measurement of the ^{63}Cu NMR quadrupolar broadening and spin-spin lattice relaxation rates at 90-10 K, Krämer and Mehring observed that the superconductor $YBa_2Cu_3O_{7\delta}$ transformed into an ordered charge density wave state at < 35 K.[28] In addition, ULT MAS NMR has been attracting interest for the study of protein systems in which the NMR signal sensitivity may be improved with the slowed down molecular motion of rapid methyl and/or amine group rotations.[29, 15, 4] Ni *et al*. reported that $^{13}CH_3$ and $^{15}NH_3$ signals in the MAS NMR spectra disappear in the temperature range of 110-80 K due to the interference of the molecular motion with the ^{1}H decoupling frequency.[15] Such methyl group rotations may also hamper the DNP efficiency, especially for samples where the ^{1}H-^{1}H spin diffusion is limited by exceedingly short ^{1}H DNP $T_{buildup}$ (e.g. 1.8 s at 86 K) found in crystalline samples with high methyl-bearing density, such as MLF (N-formyl-Met-Leu-Phe-OH).[4] Matsuki *et al*. recently found DNP enhancements of 15-fold at 27 K for MLF that yield no observable enhancements at 100 K.[4] As almost half of the proteinogenic amino acids contain CH_3 or NH_3 groups in their side chain, ULT NMR in conjunction with DNP has the potential to offer dramatic improvements for MAS NMR studies of protein samples.

In this paper, we present specifications of the newly installed JEOL ULT closed-cycle helium MAS NMR system, including helium consumption, cooling efficiency, sample temperature stability, and MAS speed stability, demonstrating that the prospect for routine operation of ULT MAS NMR is excellent. Furthermore, the MAS NMR performance at ULT was examined for a methyl-bearing NMR standard [U-^{13}C]alanine dissolved in a water/glycerol glassy matrix with different paramagnetic dopants added, including polarizing agents used for DNP at characteristic concentrations. The ^{1}H NMR signal at ULT exhibited the benefit from the enhanced Boltzmann factor at ULT, while the total experimental time is not compromised from the effective shortening of the ^{1}H spin-lattice relaxation time to a few seconds under ULT conditions. The acceleration of experimental repetition time at ULT is

achieved by exploiting the Cross Effect (two coupled electron and one nuclear spin flip) mechanism commonly used for DNP.

2. Methods

Sample preparation: 1 mg of ^{13}C uniformly labeled Alanine ([U-^{13}C]alanine, Sigma Aldrich) was added to 30 μL DNP Juice (d_8-glycerol/D_2O/H_2O = 6/3/1, v/v/v), resulting in a concentration of 375 mM [U-^{13}C]alanine, referred to as Ala henceforth. The solution was doped with paramagnetic molecules, including 10 mM AMUPol (CortecNet), 10 mM TEMTriPol-1, 20 mM 4-Amino TEMPO (Sigma Aldrich), and 14.3 mM Gd-DOTA (Macrocyclics). A volume of 30 μL of the solution was placed in the center of a 3.2 mm Si_3N_4 rotor sandwiched by Kel-F spacers. One of the Kel-F spacers was hollow and was packed with KBr for temperature calibration. In this paper, all reported temperatures are determined by measuring the spin lattice relaxation time of ^{79}Br in KBr,[30] and comparing against a calibration, unless mentioned otherwise. Specially designed Vespel caps with Dyneema fiber reinforced plastic inserts that expand at low temperatures were used to ensure the tightness of the caps at low temperatures and easy removal at room temperature.[31, 32]

Pulse sequences: The pulse sequences used for NMR experiments are shown in figure 2. ^1H NMR signal was measured using a direct $\pi/2$ pulse (figure 2A). A recycle delay of $D_1 = 7$ s was used unless mentioned otherwise. ^{13}C CP-MAS experiments were acquired using the pulse sequence shown in figure 2B. In ^{13}C CP-MAS experiments, a recycle delay of $D_1 = 7$ s was used and a Spinal64 ^1H decoupling pulse with > 80 kHz decoupling power was applied.

3. Instrumentation

ULT NMR experiments were conducted using a 600 MHz ECZ600R solid-state NMR spectrometer and a closed-cycle helium MAS system (JEOL RESONANCE Inc.). A HC double-resonance ULT MAS probe was used for the NMR experiments. The ULT MAS probe was cooled by the cold helium gas provided by the Cryovac heat exchanger (figure 1). Three Sumitomo GM

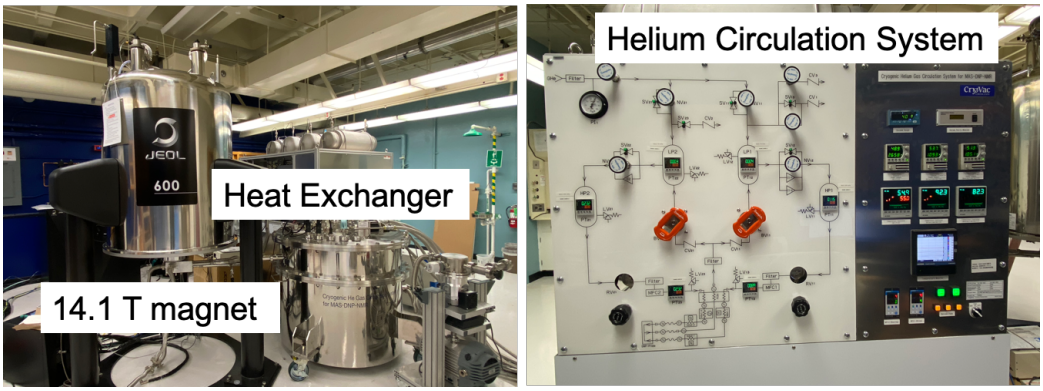

Figure 1: Left: Photo of the 14.1 T JEOL magnet and Cryovac heat exchanger unit equipped with three three Sumitomo GM cryocoolers. Right: Picture of the helium circulation unit.

Table 1: Q-factor of ^{1}H and ^{13}C RF Coils

Temperature (K)	RT	80	30
^{1}H Q-factor	243	468	709
^{13}C Q-factor	134	269	358

cryocoolers are used to cool down the helium gas in the helium circulation system. Furthermore, bellows compressors are used to provide pressurized room temperature helium gas which is later cooled down for cooling and spinning. The bearing line bellows compressor produces a maximum helium flow rate of 80 L/min and pressure of 270 kPa and drive line bellows compressor produce a maximum helium flow rate of $\sim$ 120 L/min and pressure of 270 kPa. All the helium gas flow rates in this study are measured by the normal liter per minute (NLPM) standard.

The Q-factors of the ^{1}H and ^{13}C coils were measured at variable temperatures (room temperature to 30 K) and are reported in table 1. The nutation frequencies of the ^{1}H and ^{13}C channels were also measured at different temperatures (100-26 K) and are recorded in table 2. Compared with 85 K, at 26 K both the ^{1}H and ^{13}C RF nutation frequencies increased by a factor of 1.20 and 1.13, respectively. This increase in the RF nutation frequencies is mostly due to the increase of Q-factors at low temperatures where a correlation of

Table 2: Nutation Frequencies of ^{1}H and ^{13}C RF

Temperature (K)	98	85	70	60	50	40	26
^{1}H RF 35 W (kHz)	104.2	104.2	108.7	113.6	113.6	119.0	125.0
^{13}C RF 36 W (kHz)	56.8	58.1	59.5	59.5	62.5	62.5	65.8

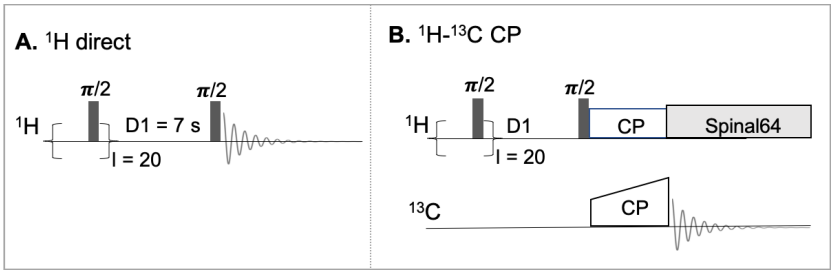

Figure 2: NMR pulse sequence used in this study for A. ^{1}H direct detection, B. ^{13}C CP-MAS.

RF field B_1 proportional to $\sqrt{Q}$ can be found.[33]

The JEOL ULT closed-cycle helium MAS system requires very little helium gas, in that there is no loss of helium during MAS NMR experiments. With the current probe design, the major source of helium gas consumption is during sample exchange. For sample exchange, the probe is detached from the heat exchanger and loaded with the sample rotor. Afterwards, the probe is connected back to the magnet and flushed with helium gas before being reattached to the heat exchanger. On average, a 7-m^3 helium gas tank allows for sample exchange >15 times.

There are two major steps to cool down the sample: heat exchanger cooling and probe cooling. During the first step, the heat exchanger is initially disconnected from the probe. Helium gas in the Cryovac heat exchanger is cooled with three Sumitomo GM cryocoolers and the temperature stabilized using internal heaters. It takes ∼4 h to cool down the heat exchanger from room temperature to < 20 K. During the sample exchange process, the temperature of the heat exchanger is maintained at the set values while disconnected from the probe. In the second step, the probe is connected back to the heat exchanger. Both the sample and probe are cooled by the cold

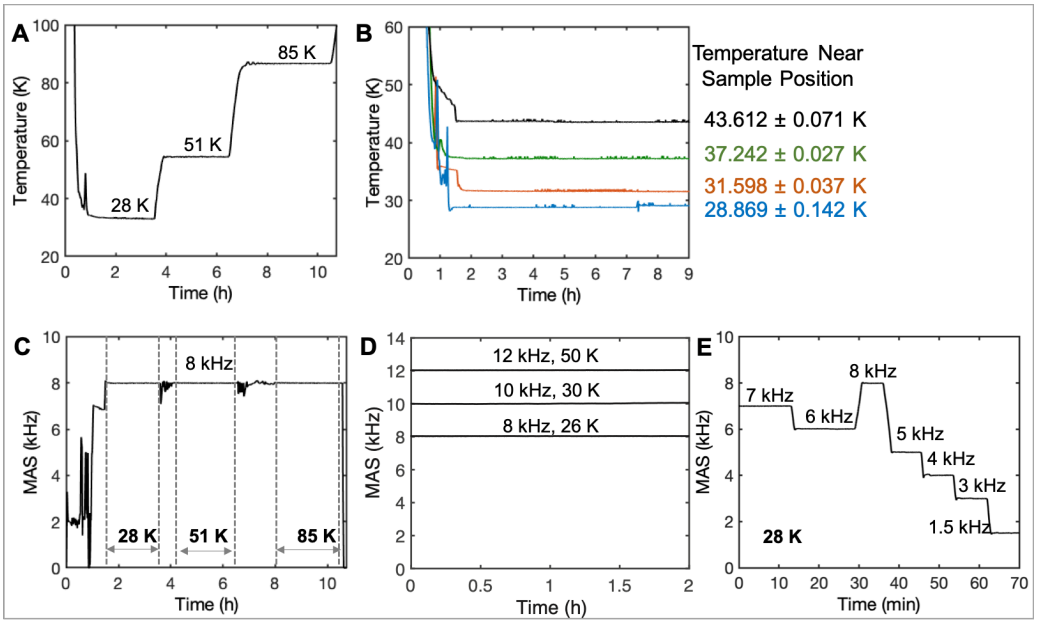

Figure 3: A. Sample temperature measured using T_1 of KBr as a function of time at set temperatures during cooling and warming. B. Temperature as measured by the sensor near the sample position as a function of time upon setting temperature and stabilization. C. MAS as a function of time at different temperatures set during spinning. D. MAS stability as a function of time at 26 K, 30 K, and 50 K. Stable MAS of 8 kHz ±3 Hz at 26 K, 10 kHz ±3 Hz at 30 K, and 12 kHz ±3 Hz at 50 K are comfortably reached. E. Changing MAS speed from 1.5 to 8 kHz with a step size of 1-1.5 kHz at 28 K.

bearing and drive helium gas provided by the heat exchanger. The sample temperature is further regulated using the heaters in the probe for bearing and drive helium gas. It took $\sim$ 1 h for the sample temperature to be brought down and stabilized at the target value after the warm probe is connected to the heat exchanger.

The efficiency of the warm-up process and sample temperature stability are discussed next. Figure 3A shows that the sample temperature, as measured by ^{79}Br T_1 of KBr, is stabilized from 28 K to 51 K within 0.5 h and from 51 K to 85 K within 1 h. Figure 3B displays temperature sensor readings at the sample position as a function of time. Upon stabilization, the sample temperature sensor reading only displays a fluctuation of ± 0.142 K over a long duration ($>$ 7 h).

The stability of sample spinning using the helium circulation system is evaluated next. Figure 3C shows that the sample maintains stable MAS at 8 kHz while changing the temperature from 28 K to both 51 K and 85 K. Further MAS stability tests were performed at different temperatures, where stable MAS frequencies of 8 kHz ± 3 Hz, 10 kHz ± 3 Hz, and 12 kHz ± 3 Hz are achieved at 26 K, 30 K, and 50 K, respectively (figure 3D). The variation in the MAS speed is calculated using standard deviation over the 2-h duration. Stable MAS at 8 kHz was maintained at 26 K for more than 10 h (experiments were terminated afterwards), as shown in SI. The helium circulation system also allows for convenient control for varying the MAS speeds as shown in figure 3E. Once the sample temperature is set, stable MAS could be readily maintained and varied from 1.5 to 8 kHz within $\sim$ 2 min of stabilizing time at each step.

It is worth noting that the reported MAS (8 kHz at 26 K, 10 kHz at 30 K, and 12 kHz at 50 K) frequencies are not the maximum values the system can reach. With the current design, the maximum achievable MAS is mainly limited by the capacity of the bellows compressors and bellows compressors with higher flow rates and pressure ratings can be attached to the helium circulation system. For reference, using the Osaka system, which is principally the same as the JEOL ULT helium circulation system, Matsuki *et al.* reported maximum MAS speeds of 12 kHz ± 5 Hz at 30 K and 14 kHz ± 5 Hz at 60 K, with stable MAS speeds maintained for days.[4] With the Grenoble system, Lee *et al.* achieved a maximum MAS of 17.5 kHz at 50 K and stable spinning at 7 kHz ± 50 Hz at 50 K. [7] The maximum helium gas flow rates available with the Grenoble system at the time of their publication[7] are: 250 L/min for bearing, 250 L/min for drive, and 500 L/min for VT.

The system testing shows that the JEOL ULT helium circulation system provides stable MAS at variable temperatures. The cooling is efficient and requires low helium consumption. The sample spinning speed is not coupled to the sample temperature, and hence can be easily stabilized at different MAS rates. A future probe designed with sample exchange capability is under construction for even more efficient cooling and less helium consumption. Next, we present studies demonstrating the benefits of conducting MAS NMR of hydrated bio-solid samples under ULT using this setup.

4. Results and discussion

4.1. ^1H NMR signal enhancement at ULT

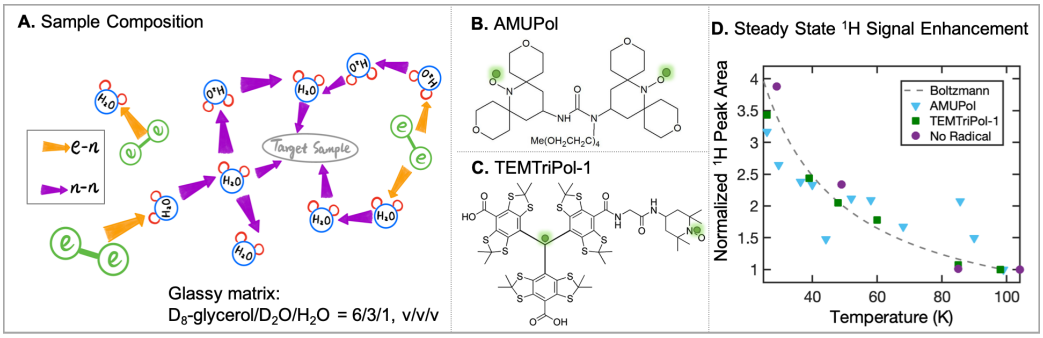

Figure 4: A. Schematics of sample composition. Coupled electron spins (e) of the bi-radicals, oxygen in H_2O, ^1H nuclei in H_2O, and target sample are represented in green, blue, red, and grey, respectively. The e-e couplings, e-n couplings, and n-n couplings are marked in green lines, yellow arrows, and purple arrows, respectively. B. Chemical structure (e is highlighted in green) of AMUPol. C. Chemical structure of TEMTriPol-1 (e is highlighted in green). D. Steady state ^1H signal intensity, normalized by the signal intensity achieved at 100 K, is plotted as a function of temperature. The ^1H NMR signal of hydrated Ala samples doped with 10 mM AMUPol (blue), 10 mM TEMTriPol-1 (green), and no radicals added (purple) are measured. Signal enhancement expected from the Boltzmann factor is calculated and plotted as the dashed grey line.

A hydrated bio-solid sample prepared for ULT NMR/DNP experiments consists of the target molecule (here Ala), a glassing matrix, and paramagnetic molecules as shown in figure 4A. In this study, a typical glassing matrix used for DNP, referred to as DNP Juice (d_8-glycerol/ D_2O/ H_2O = 6/3/1, v/v/v), is used.[3] The purpose of this sample choice is to: 1) protect the sample from freeze damage by vitrification, 2) dissolve the paramagnetic dopants, and 3) provide a spin diffusion network to achieve efficient Cross-Effect-driven ^1H T_1 relaxation (to be discussed in greater detail) and future DNP studies. We chose two bi-radicals, AMUPol and TEMTriPol-1, as the paramagnetic dopants. The chemical structures of AMUPol and TEMTriPol-1 are shown in figure 4B and 4C, respectively. The effects of relaxation enhancement by these bi-radicals will be discussed in section 4.3.

The steady state ^1H NMR signal intensity was measured in order to evaluate the signal enhancement expected from the Boltzmann factor at ULT

and RF circuit cooling. The steady state ^{1}H NMR signal of the sample was calculated as the area of the ^{1}H signal at $5 \times T_1$, where the following equation was used:

$$Area_{Steady} = Area_{D_1} \times \frac{C_1 - C_2 \times exp(-5 \times T_1/T_1)}{C_1 - C_2 \times exp(-D_1/T_1)} \quad (1)$$

In the equation, $Area_{steady}$ is the calculated NMR signal area at steady state, $Area_{D_1}$ is the measured signal area with 7-s recycle delay. $C_1 - C_2 \times exp(-\tau/T_1)$ is obtained by fitting the saturation recovery experiment at the corresponding temperature, where C_1 and C_2 are constants. Figure 4D shows the temperature-dependent steady state ^{1}H signal area normalized by that measured at 100 K. The dashed grey line is the ^{1}H NMR signal sensitivity gain expected from the Boltzmann factor alone. Normalized steady state ^{1}H NMR signals of the hydrated bio-solid samples doped with 10 mM AMUPol, 10 mM TEMTriPol-1, and no radical addition are plotted as blue, green, and purple, respectively. The steady state ^{1}H NMR signal gains at 25 K relative to 100 K for the three samples follow the Boltzmann factor, which corresponds to a signal intensity gain of $\sim$ 400 %.

The improved RF circuit's quality factors (Q) should also contribute to the ULT NMR sensitivity enhancement as the NMR signal sensitivity is proportional to $\sqrt{Q}$.[33] With the current probe, sensitivity improvements by a factor of 1.71 for ^{1}H and 2.67 for ^{13}C at 30 K compared to at room temperature, and 1.23 for ^{1}H and 1.15 for ^{13}C at 30 K compared to at 80 K are expected (table 1). The total observed ^{1}H NMR sensitivity gain is slightly lower than the product of the Boltzmann factor and Q factor gains at ULT compared to at 100 K. More studies are needed to fully delineate the reason why the full expected signal gain could not be observed. It is noteworthy that the noise levels did not change significantly between 25 K and 100 K, suggesting that the thermal noise from the RF coil is not a major factor in determining the signal-to-noise ratio of the NMR signal, but that this is instead dominated by the noise from the room-temperature preamplifier. For future development, adding and cooling a preamplifier in the probe will likely considerably increase the signal-to-noise ratio under ULT conditions.

4.2. ^{13}C CP-MAS at ULT

Next, the benefit of ULT for ^{13}C CP-MAS experiments is evaluated on a model methyl-bearing, vitrified, bio-solid sample. Ala (figure 5A) was cho-

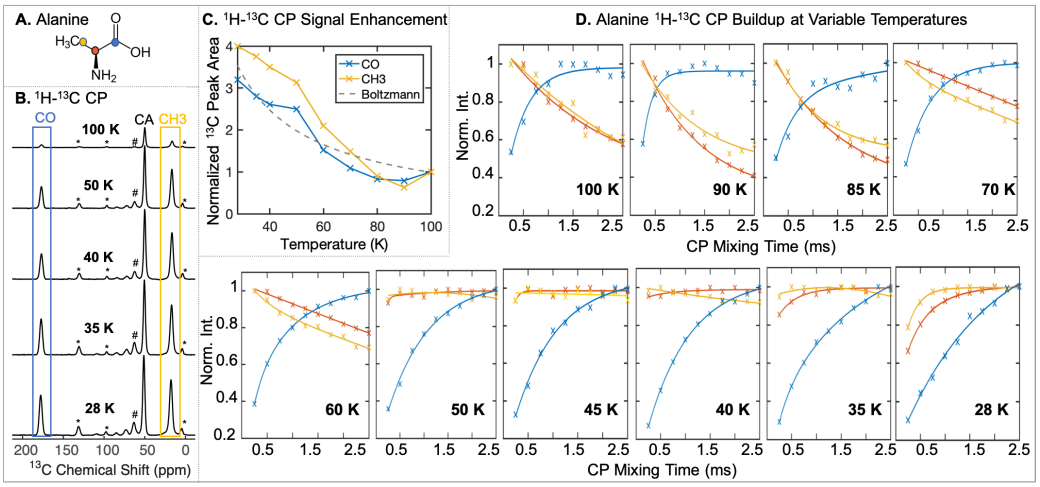

Figure 5: A. Chemical structure of Alanine, where the CO, CA, and CH_3 are marked with blue, red, and yellow dots, respectively. B. ^{13}C CP-MAS spectra of Ala at 100-28 K with CP mixing times optimized at each temperature step. Spinning side bands are marked with * and solvent glycerol peaks are marked with #. C. ^{13}C CP-MAS CO and CH_3 peak area measured at variable temperatures. CP mixing times are optimized for CO and CH_3 separately. D. Normalized signal intensities for CO, CA, and CH_3 as a function CP mixing time at variable temperatures (from 100 K to 28 K). The solution was doped with 10 mM AMUPol.

sen to probe the influence of ULT NMR on samples with CH_3 groups. ^{13}C CP-MAS measurements of vitrified Ala doped with 10 mM AMUPol are presented next, and those with different paramagnetic dopants (TEMTriPol-1, 4-Amino TEMPO, and Gd-DOTA) are shown in the SI.

Figure 5B displays the ^{13}C CP-MAS spectra of Ala measured at variable temperatures from 100 K down to 28 K, with CP mixing times optimized for each temperature. A decrease in the signal intensities for all three ^{13}C sites in Ala is observed as the sample temperature is reduced from 100 K to 28 K. Figure 5C displays the signal area of the CO (blue) and CH_3 (yellow) peaks at variable temperatures from 100 K to 28 K, where the signal intensities are normalized to that measured at 100 K. Signal enhancement expected from the Boltzmann factor is plotted in a grey dashed line. We observe a signal enhancement by 400% for the ^{13}C in the CH_3 group by lowering the sample temperature from 100 K to 28 K, which is notably higher than the increment expected from the Boltzmann factor of 357%. We ascribe the larger signal

enhancement of the methyl group ^{13}C at 28 K compared to 100 K to the improved efficiency of the CP-MAS due to reduction in methyl proton hopping rate at 28 K. At $\sim$ 80 K, we observe a significant drop in signal intensity below the expected Boltzmann factor for both CO and CH_3 sites (figure 5C). This has been previously observed and discussed by Ni *et al*. and attributed to methyl group dynamics interfering with ^1H decoupling around 110-80 K. [15]

^{13}C CP-MAS experiments of methyl-bearing bio-solids can be further optimized by the choice of CP mixing time. A series of temperature-dependent Ala ^{13}C sites' signal intensities was recorded as a function of CP mixing time and is displayed in figure 5D. The signals from CO, CA, and CH_3 sites are shown in blue, red, and yellow crosses, respectively. At 100 K, the optimum CP mixing time for the CO site is 2.5 ms while the signals for CA and CH_3 sites already started decreasing at a mixing time greater than 0.5 ms. At a temperature of 28 K, the optimum CP mixing time for all three sites has increased to greater than 1 ms for the CA and CH_3 sites and greater than 2.5 ms for the CO site. Remarkably, signals for CA and CH_3 sites did not decrease with long CP mixing time, tested up to 2.5 ms. In general, the optimum CP mixing times for the CO sites are much longer than for CH_3 sites given the weaker ^1H-^{13}C coupling in CO moieties. However, under the long spin-lock pulse required for effective CP for CO sites, the methyl protons tend to relax due to their faster relaxation rates in the RF frame ($T_{1\rho}$) at 100 K. Thus, a compromise between optimum CP for CO and methyl carbons is typically made at temperatures $>$ 50 K. However, at and below 50 K, our results (figure 5D) suggest that at CP mixing times of around 2.5 ms or longer, high CP efficiency can be achieved simultaneously for CO, CA, and CH_3. This issue is resolved because the methyl proton hopping rate is significantly slowed down at ULT.[29] In summary, operating ^{13}C CP-MAS of high methyl-bearing sample at ULT has three major benefits. First, NMR signal intensity benefits from the Boltzmann factor and enhanced Q factor of the RF circuit at ULT. Second, methyl group dynamics are dramatically slowed down at temperatures below 50 K, providing higher CP efficiency for methyl carbons. Third, optimum CP for both methyl group and non-methyl group carbons can be achieved with long CP mixing time at ULT while a compromise has to be made at higher temperatures.

4.3. ^1H T_1 spin lattice relaxation time at ULT

Table 3: ^{1}H T_1 at variable temperatures measured using ^{13}C CP-MAS saturation recovery

Temperature (K)	RT[a]	100[b]	100	85	50	30
No Radicals (s)	1.6	-	93.5	93.6	85.2	254.7
10 mM AMUPol (s)	-	4.1	5.1	5.6	5.7	5.6
10 mM TEMTriPol-1 (s)	-	1.8	2.3	2.4	2.6	3.2
20 mM 4-Amino TEMPO (s)	-	-	13.5	21.1	26.0	31.8
14.3 mM Gd-DOTA (s)	-	-	5.2	6.2	7.7	12.8

a: Measured of [U-^{13}C]alanine crystal packed in a 1 mm rotor and with a 600 MHz JEOL ULT-NMR spectrometer at a MAS frequency of 7 kHz.
b: Measured of Ala in vitrified DNP Juice in a 3.2 mm rotor of a HX probe with a 400 MHz Bruker DNP-NMR spectrometer at a MAS frequency of 7 kHz.

T_1 is another important factor that determines the NMR signal per unit experimental time. At ULT, the expectation is for the sample T_1 to be very long, leading in turn to long experimental times and low sensitivity. Generally, paramagnetic dopants are added to reduce the T_1 at ULT. In this study, the effect of AMUPol, TEMTriPol-1, 4-Amino TEMPO, and Gd-DOTA on ^{1}H T_1 relaxation enhancement was examined. The ^{1}H T_1 is measured by ^{13}C CP-MAS and the fitted values presented in table 3.

Without the addition of radical dopants, the ^{1}H T_1 increased significantly from 93.5 s to 254.7 s when the sample temperature is cooled from 100 K to 30 K. The ^{1}H T_1 of [U-^{13}C]alanine solid crystals at room temperature is provided as a reference in table 3. The addition of 10 mM AMUPol dramatically shortened the ^{1}H T_1 to $\sim$ 5-6 $\pm$ 1 s compared with the T_1 of 93.5-254.7 s without radical addition across all cryogenic temperatures tested between 100 K and 30 K. With the addition of 10 mM TEMTriPol-1 radical, the reduction of ^{1}H T_1 is even more significant and is measured to be only 2.3-3.2 s between 100 K and 30 K. Interestingly, the temperature dependency of ^{1}H T_1 appears to be low between 100 and 30 K with the addition of 10 mM AMUPol or TEMTriPol, bi-radicals widely used for CE DNP. As a comparison, with the addition of 20 mM 4-Amino TEMPO, ^{1}H T_1 increases significantly from

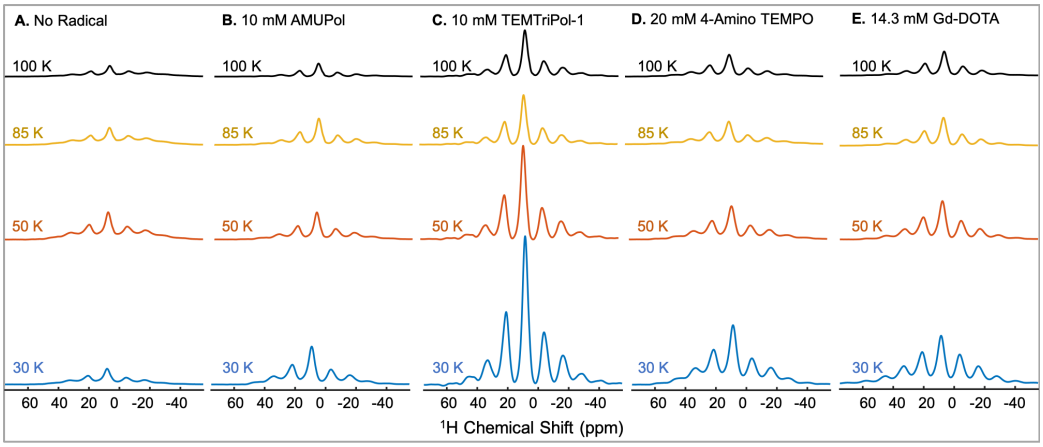

Figure 6: ^{1}H NMR spectra of the solvent ^{1}H measured at 100 K (black), 85 K (yellow), 50 K (red), and 30 K (blue) with a 600 MHz JEOL ULT-NMR system. A 7-s recycle delay was used for all the displayed spectra. Different relaxing agents are used in the solvents: A: no radicals, B: 10 mM AMUPol, C: 10 mM TEMTriPol-1, D: 20 mM 4-Amino TEMPO, and E: 14.3 mM Gd-DOTA.

13.5 s to 31.8 s from 100 K to 30 K, much longer than that measured with 10 mM bi-radical addition. This observation indicates that the *e*-*e* spin coupling is important in the mechanism that relaxes ^{1}H T_1 with the addition of bi-radical dopants. One of the most commonly assumed mechanisms for T_1 relaxation enhancement in the presence of paramagnetic dopants is the Paramagentic Relaxation Enhancement (PRE) effect. According to the theory of PRE, the nuclear spin relaxation is enhanced by external magnetic field fluctuations near the nuclear sites. In solids, the PRE rates can be modeled by the Solomon-Bloembergen-Morgan (SBM) expressions, provided in the SI. Certainly, the PRE effect and the SBM models do not include a *e*-*e* coupling term (see expression for SBM in SI), and hence predict similar effects on nuclear spin T_1 for the same global electron spin concentration. Thus, the observation that 20 mM of the monoradical 4-Amino TEMPO is dramatically less efficient compared to 10 mM of either of the two biradical dopants in reducing the ^{1}H T_1 suggests that the PRE is not the only or dominant mechanism at play.

In addition to PRE, there is another possible relaxation enhancement mechanism induced by the AMUPol radical, namely the triple-flip cross effect (CE) that commonly underlies DNP. In CE, the $\alpha_e\beta_e\alpha_n$ and $\beta_e\alpha_e\beta_n$ states

flip simultaneously during energy level crossings addressed as triple-flip in this paper. The concept of such triple-flip driven T_1 enhancement has been discussed previously, for example by Houten *et al.* in 1977.[34] They observed a significant decrease in the ^{1}H T_1 time of the (Cu,Zn)$Cs_2(SO_4)_2{\cdot}6(H,D)_2O$ crystal whenever the rotating crystal orientation provided EPR frequencies that matched the simultaneous triple-flip condition $\omega_{e1} - \omega_{e2} = \omega_{1H}$. Such matching condition is also the most commonly relied upon mechanism for DNP. The triple-flip driven nuclear T_1 relaxation enhancement mechanism was also later investigated by Leavesley *et al.*, where ^{1}H T_1 was measured for glycerol-water mixture doped with a series of mono-, bi-, tri-, and dendritic-nitroxide radicals.[35] They observed that a stronger *e*-*e* coupling leads to a shorter solvent ^{1}H T_1, suggesting that the ^{1}H T_1 relies on coupled electron spin flip.

When considering both the theory of PRE and triple-flip processes in CE DNP, we can reconcile our observation that the ^{1}H T_1 measured with Ala sample doped with AMUPol is shorter than that with 4-Amino TEMPO dopants and remains virtually unchanged between 100 k and 30 K. As the temperature dependent electron spin lattice relaxation rate has an impact on the PRE efficiency and negligible impact on the simultaneous triple-flip CE rate, ^{1}H T_1 enhanced via triple-flip CE mechanism has less temperature dependency compared with PRE. In other words, both PRE and triple flip effects coexist and contribute to ^{1}H T_1 enhancements. Still, the triple-flip CE is the dominant mechanism of shortening the ^{1}H T_1 at ULT, as manifested in the elimination of any temperature dependence of ^{1}H T_1 at ULT.

We further explored the influence of the efficiency of the triple-flip CE mechanism on enhancing the nuclear T_1. As we discussed earlier, ^{1}H T_1 of a sample doped with 10 mM TEMTriPol-1 is shorter than that doped with 10 mM AMUPol at different temperatures 100-30 K and at two different fields 14.1 T and 9.4 T. It is known that the efficiency of the *e*-*e*-^{1}H triple-flip CE is much greater with the TEMTriPol-1 radical compared to AMUPol.[36, 37] This effect has also been modeled by Equbal *et al.*.[38] Our observation suggests that higher triple-flip efficiency leads to more ^{1}H T_1 relaxation enhancement. This further corroborates our conclusion that the triple-flip CE is the dominant nuclear T_1 relaxation mechanism under ULT conditions with bi-radical addition.

The effect of a typical PRE dopant, Gd-DOTA, at 14.3 mM concentration is examined to further explore the benefit of using the triple-flip mechanism for nuclear T_1 enhancement rather than relying on the PRE. The choice of the Gd-DOTA radical concentration is determined based on the study from Ullrich *et al.*.[39] It has been already established that the solvent T_1 depends on the total Gd-DOTA concentration. In order to result in a ^{1}H T_1 of 5.1 s at 100 K, same as that measured with 10 mM AMUPol dopants, a Gd-DOTA concentration of 14.3 mM was added based on the calculation provided by Ullrich *et al.*.[39] Experimentally, we measured at 100 K a ^{1}H T_1 of 5.2 s of an Ala sample in DNP Juice doped with 14.3 mM Gd-DOTA, i.e. remarkably close to the predicted value. At 30 K, the ^{1}H T_1 significantly increases to 12.8 s, longer than that of samples doped with 10 mM AMUPol (5.6 s) at the same temperature. This observation highlights the potential dominance and benefit of CE-driven nuclear spin T_1 relaxation enhancement at ULT condition for NMR with or without DNP.

Next, we compare the ^{1}H NMR signals of all five Ala samples in vitrified DNP Juice with no or different paramagnetic dopants added, shown in figure 6. The spectra were acquired using $D_1 = 7$ s and 4 scans. This comparison takes into account all of the factors that can enhance/attenuate NMR signal intensity, such as Boltzmann factor, Q factor, T_1, paramagnetic quenching,[40], as well as the depolarization effect.[41, 42, 22] Among the samples, Ala solution doped with TEMTriPol-1 clearly and by far yields the highest NMR signal intensity across a range of cryogenic temperatures from 100 K to 30 K. This observation suggests that TEMTriPol-1 is not only a radical that can provide high CE DNP enhancement[37, 36], but is also an excellent nuclear T_1 relaxation enhancing paramagnetic dopant that shows less impairment in the NMR signal quality compared to AMUPol.

4.4. ^{13}C CP-MAS NMR Spectral Linewidth at ULT

The NMR spectral resolution is another critical factor in bio-solid NMR applications, and of concern at ULT. In this paper, the spectral resolution is evaluated by the full width at half maximum (FWHM) of the CH_3 peak measured using ^{13}C CP-MAS, as recorded in table 4. FWHM of the CA and CO peaks are recorded in the SI. Without radical addition, as temperature decreases from 100 K to 30 K, FWHM of ^{13}C signal in CH_3 increases from

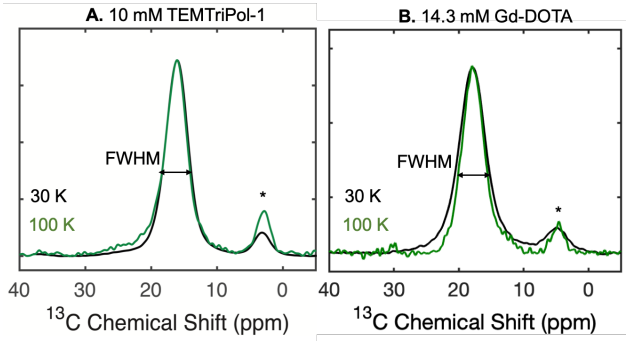

Figure 7: ^{13}C CP-MAS of CH_3 in Ala measured at 30 K (black) and 100 K (green) with the addition of paramagnetic dopants: A: 10 mM TEMTriPol-1, B: 14.3 mM Gd-DOTA. The spinning side bands were marked in *.

Table 4: CH_3 Peak Full Width at Half Maximum (FWHM) at Variable Temperatures Measured Using ^{13}C CP-MAS (20 Hz line broadening was applied)

Temperature (K)	100[a]	100	85	50	30
No Radicals (ppm)	-	3.3	4.3	3.7	3.9
10 mM AMUPol (ppm)	4.7	3.8	4.5	3.8	4.0
10 mM TEMTriPol-1 (ppm)	4.6	3.7	4.5	3.7	4.0
20 mM 4-Amino TEMPO (ppm)	-	3.6	3.8	3.9	4.2
14.3 mM Gd-DOTA (ppm)	-	4.0	4.9	4.4	4.8

a: Measured with a 3.2 mm HX probe using a 400 MHz Bruker DNP-NMR spectrometer at a MAS frequency of 7 kHz.

3.3 ppm to 3.9 ppm. It is worth mentioning that the FWHM of the ^{13}C signal of the same sample, measured under identical conditions except at 85 K, increased to 4.3 ppm, which is a likely from interference between the methyl group rotation frequency and the ^{1}H decoupling, as already discussed in the literature previously.[15] As a comparison, FWHM of CA and CO ^{13}C signal increased while temperature was cooled down from 100 K to 30 K. With the addition of 10 mM AMUPol, the FWHM of CH_3 peak at 100 K increases by 0.5 ppm compared with no radical addition, while at 30 K the FWHM only increases by 0.1 ppm. Compared with the FWHM without radical dopants, the CH_3 peak line broadening with the addition of 10 mM AMUPol is in-

significant at 30 K. Surprisingly, upon adding 10 mM AMUPol, FWHM of CO peak decreased by 0.2 ppm at 100 K and 0.5 ppm at 30 K (table S2, SI). The reason why the linewidth of the CO peak decreased with CE radical addition is still not understood.

The FWHM does not change when 10 mM TEMTriPol-1 is used as the paramagnetic dopants, across all cryogenic temperatures tested as compared with that measured with 10 mM AMUPol addition. This suggests that the increase in the triple-flip CE efficiency does not increase the NMR spectral linewidth further. When 20 mM 4-Amino TEMPO is used as the paramagnetic dopants, the FWHM increases from 3.6 ppm at 100 K to 4.2 ppm at 30 K, which is much larger compared with the FWHM measured without radical addition. The increase in linewidth at ULT compared to at 100 K is even more severe when the sample is doped with the commonly used PRE agent Gd-DOTA, where the FWHM increases from 4.0 ppm at 100 K to 4.8 ppm at 30 K. Figure 7 shows the overlaid normalized ^{13}C CP-MAS spectra of CH_3 in Ala measured at 30 K (black) and 100 K (green), with the effect of line broadening of samples doped with TEMTriPol-1 (figure 7A) compared with that doped with Gd-DOTA (figure 7B) shown side by side. The spectral linewidth of the CH_3 peak shows a more significant increase when doped with Gd-DOTA compared with TEMTriPol-1. This observation suggests that the PRE agent might cause more severe line broadening compared with paramagnetic dopants optimized for triple-flip CE. This is likely because the PRE shortens both the nuclear T_1 and T_2, while the triple-flip CE is optimized to enhance longitudinal spin flips, and hence mainly shortens T_1. This is another great advantage of the reliance on paramagnetic molecules optimized to perform triple-flip CE as the paramagentic centers for ULT NMR experiments. However, more rigorous examination is needed to gain a mechanistic understanding of the line broadening effects from PRE and the triple-flip mechanism.

5. Conclusion

In conclusion, the JEOL 600 MHz closed-cycle helium MAS system has allowed efficient cooling and stable spinning (tested from 1.5 kHz to 12 kHz) under variable temperatures (tested from 25 K to 105 K) with minimal helium consumption, mainly from sample exchange. Using this system, we

have systematically examined the NMR properties of a hydrated bio-solid, [U-^{13}C]alanine (Ala) dissolved in d_8-glycerol/D_2O /H_2O (DNP Juice) solution doped with paramagnetic dopants at ULT. Steady state ^{1}H NMR signal at ULT has shown a similar signal intensity increment compared with the Boltzmann factor. The NMR signal sensitivity of hydrated and vitrified biosolids at ULT is enhanced by several factors: the Boltzmann factor, the increase in the quality factor of the RF circuitry, and the reduction of methyl group rotation rate. At 28 K, the ^{13}C CP-MAS signal for the methyl ^{13}C in Ala achieved a signal enhancement of 400% compared with signal at 100 K, which is higher than the contribution from the Boltzmann factor (357%). This signal enhancement is ascribed to the improved efficiency of CP due to the reduction in methyl proton hopping rate. In addition, at ULT, an optimum CP mixing time can be chosen to achieve high CP efficiency for both CO and CH_3 carbons, while a compromise has to be found for the CP mixing tine at higher temperatures (> 50 K).

Our study also highlights a major benefit of paramagnetic dopants commonly used for CE DNP for ULT NMR operation, with or without DNP. The ^{1}H T_1 enhancement is most significant in the presence of paramagnetic dopants known to display efficient triple-flip CE and at concentrations typically used for DNP. For example, the ^{1}H T_1 shortens from 254.7 s at 30 K to 3.2 s at 30 K with the addition of 10 mM TEMTriPol-1, known to provide efficient CE DNP enhancement at high field and under fast MAS. The efficient T_1 relaxation enhancement with TEMTriPol-1 is only in part due to paramagnetic relaxation enhancement (PRE) effects, but dominantly due to efficient *e*-*e*-^{1}H triple-flip processes that, in turn, drives nuclear T_1 relaxation. Critically, the linewidths of the ^{13}C CP-MAS spectra for Ala doped with triple-flip radicals are not further impeded at ULT compared with that at 100 K, suggesting that the prospects for NMR and DNP under ULT conditions are excellent. This study also provides a promising design principle for developing paramagnetic dopants to achieve high nuclear spin lattice relaxation enhancement, especially at cryogenic temperatures. In fact, the measurement of nuclear T_1 enhancement offers insight into developing samples and conditions favorable for achieving CE DNP.

6. Acknowledgments

We thank JEOL RESONANCE Inc., Japan; JEOL USA Inc.; and Cryovac Corp., Japan, for closely collaborating with us on the installation of the 14.1 T JEOL NMR instrument with a closed-cycle helium MAS system. We would like to thank especially Mr. Hiroto Suematsu from JEOL RESONANCE Inc., Japan for the generous customer support and technology development. We would like to thank the Department of Chemistry and Biochemistry at the University of California Santa Barbara for providing the lab space and policies that allowed for this successful installation during the COVID-19 pandemic. We would like to thank Prof. Yangping Liu at the School of Pharmacy, Tianjin Medical University, Tianjin, China, for synthesizing and providing the TEMTriPol-1 radical. This work was supported by the National Science Foundation Grant CHE CMI #2004217.

7. Supporting Information

Supporting information on more NMR experiments is available free of charge at DOI: XXX.

References

[1] K. Hashi, S. Ohki, S. Matsumoto, G. Nishijima, A. Goto, K. Deguchi, K. Yamada, T. Noguchi, S. Sakai, M. Takahashi, et al., Achievement of 1020 mhz nmr, Journal of Magnetic Resonance 256 (2015) 30–33.

[2] M. Callon, A. A. Malär, S. Pfister, V. Římal, M. E. Weber, T. Wiegand, J. Zehnder, M. Chávez, R. Cadalbert, R. Deb, et al., Biomolecular solid-state nmr spectroscopy at 1200 mhz: the gain in resolution, Journal of Biomolecular NMR (2021) 1–18.

[3] D. A. Hall, D. C. Maus, G. J. Gerfen, S. J. Inati, L. R. Becerra, F. W. Dahlquist, R. G. Griffin, Polarization-enhanced nmr spectroscopy of biomolecules in frozen solution, Science 276 (1997) 930–932.

[4] Y. Matsuki, T. Sugishita, T. Fujiwara, Surface-only spectroscopy for diffusion-limited systems using ultra-low-temperature dnp mas nmr at 16.4 t, The Journal of Physical Chemistry C 124 (2020) 18609–18614.

[5] K. R. Thurber, W.-M. Yau, R. Tycko, Low-temperature dynamic nuclear polarization at 9.4 t with a 30 mw microwave source, Journal of Magnetic Resonance 204 (2010) 303–313.

[6] F. J. Scott, N. Alaniva, N. C. Golota, E. L. Sesti, E. P. Saliba, L. E. Price, B. J. Albert, P. Chen, R. D. O'Connor, A. B. Barnes, A versatile custom cryostat for dynamic nuclear polarization supports multiple cryogenic magic angle spinning transmission line probes, Journal of Magnetic Resonance 297 (2018) 23–32.

[7] D. Lee, E. Bouleau, P. Saint-Bonnet, S. Hediger, G. De Paëpe, Ultra-low temperature mas-dnp, Journal of Magnetic Resonance 264 (2016) 116–124.

[8] Y. Matsuki, T. Kobayashi, J. Fukazawa, F. A. Perras, M. Pruski, T. Fujiwara, Efficiency analysis of helium-cooled mas dnp: case studies of surface-modified nanoparticles and homogeneous small-molecule solutions, Physical Chemistry Chemical Physics 23 (2021) 4919–4926.

[9] K. Thurber, R. Tycko, Low-temperature dynamic nuclear polarization with helium-cooled samples and nitrogen-driven magic-angle spinning, Journal of Magnetic Resonance 264 (2016) 99–106.

[10] B. Huggins, P. D. Ellis, Aluminum-27 nuclear magnetic resonance study of aluminas and their surfaces, Journal of the American Chemical Society 114 (1992) 2098–2108.

[11] M. Concistrè, E. Carignani, S. Borsacchi, O. G. Johannessen, B. Mennucci, Y. Yang, M. Geppi, M. H. Levitt, Freezing of molecular motions probed by cryogenic magic angle spinning nmr, The journal of physical chemistry letters 5 (2014) 512–516.

[12] K. R. Thurber, R. Tycko, Perturbation of nuclear spin polarizations in solid state nmr of nitroxide-doped samples by magic-angle spinning without microwaves, The Journal of chemical physics 140 (2014) 05B608_1.

[13] H.-Y. Chen, R. Tycko, Temperature-dependent nuclear spin relaxation due to paramagnetic dopants below 30 k: Relevance to dnp-enhanced magnetic resonance imaging, The Journal of Physical Chemistry B 122 (2018) 11731–11742.

[14] T. Sugishita, Y. Matsuki, T. Fujiwara, Absolute 1h polarization measurement with a spin-correlated component of magnetization by hyperpolarized mas-dnp solid-state nmr, Solid state nuclear magnetic resonance 99 (2019) 20–26.

[15] Q. Z. Ni, E. Markhasin, T. V. Can, B. Corzilius, K. O. Tan, A. B. Barnes, E. Daviso, Y. Su, J. Herzfeld, R. G. Griffin, Peptide and protein dynamics and low-temperature/dnp magic angle spinning nmr, The Journal of Physical Chemistry B 121 (2017) 4997–5006.

[16] A. N. Smith, K. Märker, T. Piretra, J. C. Boatz, I. Matlahov, R. Kodali, S. Hediger, P. C. van der Wel, G. De Paëpe, Structural fingerprinting of protein aggregates by dynamic nuclear polarization-enhanced solid-state nmr at natural isotopic abundance, Journal of the American Chemical Society 140 (2018) 14576–14580.

[17] A. N. Smith, M. A. Caporini, G. E. Fanucci, J. R. Long, A method for dynamic nuclear polarization enhancement of membrane proteins, Angewandte Chemie 127 (2015) 1562–1566.

[18] V. Macho, R. Kendrick, C. Yannoni, Cross polarization magic-angle spinning nmr at cryogenic temperatures, Journal of Magnetic Resonance (1969) 52 (1983) 450–456.

[19] A. Hackmann, H. Seidel, R. Kendrick, P. Myhre, C. Yannoni, Magic-angle spinning nmr at near-liquid-helium temperatures, Journal of Magnetic Resonance (1969) 79 (1988) 148–153.

[20] A. Samoson, T. Tuherm, J. Past, A. Reinhold, T. Anupõld, I. Heinmaa, New horizons for magic-angle spinning nmr, New Techniques in Solid-State NMR (2005) 15–31.

[21] M. Concistrè, O. G. Johannessen, E. Carignani, M. Geppi, M. H. Levitt, Magic-angle spinning nmr of cold samples, Accounts of chemical research 46 (2013) 1914–1922.

[22] A. Lund, A. Equbal, S. Han, Tuning nuclear depolarization under mas by electron t 1e, Physical Chemistry Chemical Physics 20 (2018) 23976–23987.

[23] E. Bouleau, P. Saint-Bonnet, F. Mentink-Vigier, H. Takahashi, J.-F. Jacquot, M. Bardet, F. Aussenac, A. Purea, F. Engelke, D. Hediger, Sabine Lee, G. De Paëpe, Pushing nmr sensitivity limits using dynamic nuclear polarization with closed-loop cryogenic helium sample spinning, Chemical science 6 (2015) 6806–6812.

[24] Y. Matsuki, S. Nakamura, S. Fukui, H. Suematsu, T. Fujiwara, Closed-cycle cold helium magic-angle spinning for sensitivity-enhanced multi-dimensional solid-state nmr, Journal of Magnetic Resonance 259 (2015) 76–81.

[25] Y. Matsuki, T. Idehara, J. Fukazawa, T. Fujiwara, Advanced instrumentation for dnp-enhanced mas nmr for higher magnetic fields and lower temperatures, Journal of Magnetic Resonance 264 (2016) 107–115.

[26] Y. Matsuki, T. Fujiwara, Cryogenic platforms and optimized dnp sensitivity, eMagRes (2018) 9–24.

[27] Y. Matsuki, T. Fujiwara, Advances in high-field dnp methods, in: Experimental Approaches of NMR Spectroscopy, Springer, 2018, pp. 91–134.

[28] S. Krämer, M. Mehring, Low-temperature charge ordering in the superconducting state of $yba_2cu_3o_{7\delta}$, Physical review letters 83 (1999) 396.

[29] S. Clough, J. Hill, Temperature dependence of methyl group tunnelling rotation frequency, Journal of Physics C: Solid State Physics 7 (1974) L20.

[30] K. R. Thurber, R. Tycko, Measurement of sample temperatures under magic-angle spinning from the chemical shift and spin-lattice relaxation rate of 79br in kbr powder, Journal of magnetic resonance 196 (2009) 84–87.

[31] Y. Endo, T. Fujiwara, Y. Matruki, S. Nakamura, T. Nemoto, Nmr sample tube, U.S. Patent US10914799B2, Feb. 2021.

[32] Y. Endo, T. Fujiwara, Y. Matruki, S. Nakamura, T. Nemoto, Nmr sample tube, Japanese Patent JP6750819B2, Sep. 2020.

[33] F. D. Doty, Probe design and construction, Encyclopedia of NMR 6 (1996) 3753–3762.

[34] J. Van Houten, W. T. Wenckebach, N. Poulis, Proton spin-lattice relaxation in deuterated diluted copper tutton salts, Physica B+ C 92 (1977) 201–209.

[35] A. Leavesley, S. Jain, I. Kamniker, H. Zhang, S. Rajca, A. Rajca, S. Han, Maximizing nmr signal per unit time by facilitating the e–e–n cross effect dnp rate, Physical Chemistry Chemical Physics 20 (2018) 27646–27657.

[36] F. Mentink-Vigier, G. Mathies, Y. Liu, A.-L. Barra, M. A. Caporini, D. Lee, S. Hediger, R. G. Griffin, G. De Paëpe, Efficient cross-effect dynamic nuclear polarization without depolarization in high-resolution mas nmr, Chemical science 8 (2017) 8150–8163.

[37] G. Mathies, M. A. Caporini, V. K. Michaelis, Y. Liu, K.-N. Hu, D. Mance, J. L. Zweier, M. Rosay, M. Baldus, R. G. Griffin, Efficient dynamic nuclear polarization at 800 mhz/527 ghz with trityl-nitroxide biradicals, Angewandte Chemie International Edition 54 (2015) 11770–11774.

[38] A. Equbal, K. Tagami, S. Han, Balancing dipolar and exchange coupling in biradicals to maximize cross effect dynamic nuclear polarization, Physical Chemistry Chemical Physics 22 (2020) 13569–13579.

[39] S. J. Ullrich, S. Hölper, C. Glaubitz, Paramagnetic doping of a 7tm membrane protein in lipid bilayers by gd^{3+}-complexes for solid-state nmr spectroscopy, Journal of biomolecular NMR 58 (2014) 27–35.

[40] B. Corzilius, L. B. Andreas, A. A. Smith, Q. Z. Ni, R. G. Griffin, Paramagnet induced signal quenching in mas–dnp experiments in frozen homogeneous solutions, Journal of Magnetic Resonance 240 (2014) 113–123.

[41] Y. Hovav, I. Kaminker, D. Shimon, A. Feintuch, D. Goldfarb, S. Vega, The electron depolarization during dynamic nuclear polarization: measurements and simulations, Physical Chemistry Chemical Physics 17 (2015) 226–244.

[42] F. Mentink-Vigier, S. Paul, D. Lee, A. Feintuch, S. Hediger, S. Vega, G. De Paëpe, Nuclear depolarization and absolute sensitivity in magic-angle spinning cross effect dynamic nuclear polarization, Physical Chemistry Chemical Physics 17 (2015) 21824–21836.